Traffic

WILEY

Traffic

RESEARCH ARTICLE OPEN ACCESS

Mechanistic Insights Into an Ancient Adenovirus Precursor Protein VII Show Multiple Nuclear Import Receptor Pathways

Sepehr Nematollahzadeh[1] | Ajani Athukorala[2] | Camilla M. Donnelly[3,4] | Silvia Pavan[1] | Victoria Atelie-Djossou[1] | Enzo Di Iorio[1] | Babu Nath[3] | Karla J. Helbig[2] | Brian P. McSharry[3,4] | Jade K. Forwood[3,4] | Subir Sarker[2,5,6] | Gualtiero Alvisi[1]

[1]Department of Molecular Medicine, University of Padua, Padua, Italy | [2]Department of Microbiology, Anatomy, Physiology, and Pharmacology, School of Agriculture, Biomedicine and Environment, La Trobe University, Melbourne, Victoria, Australia | [3]School of Dentistry and Medical Sciences Biomedical Sciences, Charles Sturt University, Wagga Wagga, New South Wales, Australia | [4]Gulbali Institute, Charles Sturt University, Wagga Wagga, New South Wales, Australia | [5]Biomedical Sciences and Molecular Biology, College of Public Health, Medical and Veterinary Sciences, James Cook University, Townsville, Queensland, Australia | [6]Australian Institute of Tropical Health and Medicine, James Cook University, Townsville, Queensland, Australia

Correspondence: Subir Sarker (subir.sarker@jcu.edu.au) | Gualtiero Alvisi (gualtiero.alvisi@unipd.it)

Received: 5 February 2024 | **Revised:** 10 July 2024 | **Accepted:** 30 July 2024

Funding: S.S. is the recipient of an Australian Research Council (grant number DE200100367) funded by the Australian Government. A.A. is supported by La Trobe University (LTU) under the LTU Graduate Research Scholarship and LTU Full Fee Research Scholarship. The funders had no role in the design of the study; in the collection, analyses, or interpretation of data; in the writing of the manuscript, or in the decision to publish the results. C.M.D. is a THRIIVE postdoctoral fellow.

Keywords: genome packaging | NLS | nuclear entry | nucleolar localization signal (NoLS) | Pre-pVII | siadenovirus | transportin-1

ABSTRACT

Adenoviral pVII proteins are multifunctional, highly basic, histone-like proteins that can bind to and transport the viral genome into the host cell nucleus. Despite the identification of several nuclear localization signals (NLSs) in the pVII protein of human adenovirus (HAdV)2, the mechanistic details of nuclear transport are largely unknown. Here we provide a full characterization of the nuclear import of precursor (Pre-) pVII protein from an ancient siadenovirus, frog siadenovirus 1 (FrAdV1), using a combination of structural, functional, and biochemical approaches. Two strong NLSs (termed NLSa and NLSd) interact with importin (IMP)β1 and IMPα, respectively, and are the main drivers of nuclear import. A weaker NLS (termed NLSb) also contributes, together with an additional signal (NLSc) which we found to be important for nucleolar targeting and intranuclear binding. Expression of wild-type and NLS defective derivatives Pre-pVII in the presence of selective inhibitors of different nuclear import pathways revealed that, unlike its human counterpart, FrAdV1 Pre-pVII nuclear import is dependent on IMPα/β1 and IMPβ1, but not on transportin-1 (IMPβ2). Clearly, AdVs evolved to maximize the nuclear import pathways for the pVII proteins, whose subcellular localization is the result of a complex process. Therefore, our results pave the way for an evolutionary comparison of the interaction of different AdVs with the host cell nuclear transport machinery.

Abbreviations: %, percent sign; °C, celsius; Å, angstrom; β-gal, β-galactosidase; μL, microliter; μm, micrometer; μM, micromolar; AdV, adenovirus; ANOVA, analysis of variance; BAdV, bovine adenovirus; CLSM, confocal laser scanning microscopy; DNA, deoxyribonucleic acid; dsDNA, double-stranded DNA; DTT, dithiothreitol; EE, early endosome; Fb, background fluorescence; Fc, cytoplasmic fluorescence; FITC, fluorescein isothiocyanate; Fn, nuclear fluorescence; Fno, nucleolar fluorescence; FP, fluorescence polarisation; FPLC, fast protein liquid chromatography; FrAdV1, frog siadenovirus 1; GFP, green fluorescent protein; HAdV, Human adenovirus; HCMV, human cytomegalovirus; IMP, importin; importin 4, Ran-binding protein 4; importin 5, karyopherin β3; importin 7, Ran binding protein 7; IMPβ2, transportin-1; kDa, kilo dalton; LTA, large tumor antigen; mg, milligram; min, minute; mL, milliliter; mM, millimolar; MWCO, molecular weight cut-off; MX2, high-flux undulator microfocus beamline; NLS, nuclear localization signal; nc, non-classical; NPC, nuclear pore complex; ng, nanograms; nM, nanomolar; nm, nanometer; pH, potential of hydrogen; pVII, protein VII; Pre-pVII, precursor protein VII; PsSiAdV, psittacine siadenovirus F; PBS, phosphate-buffered saline; PDB, Protein Data Bank; rpm, revolutions per minute; RT, room temperature; SD, standard deviation; SDS-PAGE, sodium dodecyl-sulfate polyacrylamide gel electrophoresis; SV, Simian vacuolating virus; U/mL, units per milliliter; V, volt; v/v, volume per volume.

Sepehr Nematollahzadeh and Ajani Athukorala are joint first authors.

1 | Introduction

Adenoviruses (AdVs) are an intensively studied group of viruses due to their remarkable diversity, pathogenic relevance, and prominent role as leading candidates as viral vectors in gene therapy. AdVs are classified into six genera: *Mastadenovirus*, *Aviadenovirus*, *Atadenovirus*, *Siadenovirus*, *Ichtadenovirus*, and *Testadenovirus*, and their infections have been reported in almost all vertebrates. *Siadenovirus*, in particular, is known for its distinctive genomic characteristics, has been identified from reptiles and avian species, and is proposed to have an amphibian origin [1–5]. Frog siadenovirus 1 (FrAdV1), identified in the northern leopard frog (*Lithobates pipiens*), was the first siadenovirus to be sequenced [1] and serves as the common ancestor for all siadenoviruses. However, despite extensive investigations, no further evidence of FrAdV1 infections in frogs or any other animal has been uncovered [6]. The evolution of adenoviruses with an amphibian origin to infect distantly related host species, including critically endangered bird species, emphasizes potential host-switching [7]. Their initial detection in a cell line of reptilian origin and the absence of further evidence concerning frog siadenoviruses presents them as a compelling area of study.

During AdV infection, viral fiber and penton proteins bind and interact with the coxsackie adenoviral receptor and integrin V, respectively, triggering virus uptake into clathrin-coated early endosomes (EEs) [7–10]. In the EE, a drop in the pH induces conformational changes in the capsid and facilitates the release of the proteins VI and penton, disrupting the endosomal membrane, thus allowing the release and translocation of nucleocapsid to the nucleus in a microtubule and dynein-dependent fashion [11]. The capsid consists of three cationic proteins termed protein V, VII, and mu, with protein VII (pVII) being the most abundant. Precursor protein VII (Pre-pVII) is expressed in the late phase of infection and processed by the adenoviral protease upon virus assembly. Pre-pVII is cleaved by the adenoviral protease, which removes 24 amino acid residues from the *N*-terminus, resulting in mature pVII [11].

Adenovirus pVII is a highly basic protein due to the presence of arginine and lysine residues and can be considered as functional analogs of histones, condensing the viral genome to be positioned inside the viral particle, with mature pVII being involved in nuclear delivery of viral DNA upon infection of new cells [10]. Accordingly, both pVII and Pre-pVII are endowed with nuclear targeting abilities during viral infection [8, 10, 12, 13].

Molecules smaller than 70 kDa can passively diffuse through the nuclear pore complex (NPC; [14]). On the other hand, larger ones and those which need to quickly accumulate in the cell nucleus require energy dependent transport, mediated by cellular transporters belonging to the importin (IMP) superfamily, which recognize nuclear localization signals (NLSs) on cargoes [14, 15]. Several IMPs have been described in eukaryotes, and despite their exact number varies in different organisms, most of them are highly conserved [16]. Although clear rules determining the specific interaction between most IMPs and their cargos are still lacking, it is becoming increasingly clear that each IMP is endowed with peculiar cargo recognition properties, which have only been partially characterized [17]. So far, four types of NLSs have been described, each being recognized by specific IMPs [18]. The best characterized NLS are termed "classical" (c)NLS and are short sequences enriched in basic amino acids such as arginine and lysine [19]. cNLSs can either be monopartite, consisting of a single stretch of basic amino acids, or consist of two basic sequences separated by a short linker in a bipartite arrangement [20–22]. cNLSs directly interact with IMPα, which functions as an adapter bridging the cargo to IMPβ1, which in turn mediates translocation of the complex across the NPC. Nonclassical (nc)NLSs, on the other hand, are able to bind directly to IMPβ1 or one of its several orthologs such as transportin-1 (IMPβ2), Ran-binding protein 4 (importin 4), karyopherin β3 (importin 5), Ran-binding protein 7 (importin 7), and many others without the need for IMPα [17, 19, 23, 24].

Directionality of nuclear transport is warranted by the presence of a profound difference between GDP and GTP concentrations in different cellular compartments. Although GDP is highly enriched in the cytosol, GTP is particularly abundant in the nucleus [25]. After cargo:IMPs complexes are translocated in the nucleoplasm, interaction of IMPβ1 or its orthologs with Ran:GTP induces a conformational change that results in cargo release [26], whereas IMPs are recycled back to the cytosol to be engaged in new rounds of nuclear import.

In recent years, several studies have investigated the structural, functional, and cellular properties of human adenovirus (HAdV) pVII and began the characterization of its nuclear targeting abilities [27]. HAdV pVII proteins are able to interact with cellular components such as IMP7, IMPβ2, IMPα/β1, hsp70, and histone H1 and are, therefore, believed to use multiple nuclear import pathways [8, 10, 12]. Furthermore, HAdV Pre-VII and pVII appear to have different nuclear import preferences, with cleavage believed to alter its IMPs interaction properties. Indeed, although pVII preferentially interacts with IMPβ2, Pre-pVII has a higher affinity for IMPα/β1 [12]. Unfortunately, despite several NLSs have been described within pVII, their contribution to nuclear transport is still not fully elucidated, and the molecular determinants of nuclear import are not completely characterized [8, 10, 12]. In addition, little is known regarding nuclear import of adenoviruses of animal origin, including siadenoviruses, with the exception of very recent reports from psittacine siadenovirus F (PsSiAdV) and bovine adenovirus (BAdV)-3 [13, 28]. To address this issue, we thoroughly characterized the nuclear import process of Pre-pVII from FrAdV1, which can be considered the most ancient member of the *Siadenovirus* genus. We identified four putative NLSs and characterized their structural, functional, and biochemical properties utilizing a wide range of approaches, dissecting the contribution of each to Pre-VII subcellular localization. Upon expression in mammalian cells in the absence of any other viral protein, GFP and GFP-β-galactosidase (β-gal) Pre-pVII fusion proteins strongly accumulated in the nucleolus. The subcellular localization of several full-length Pre-pVII derivatives carrying amino acid substitutions within key NLSs basic residues revealed that a total impairment on nuclear localization was detected only upon inactivation of all NLSs, whereas co-expression with selective nuclear transport inhibitors highlighted an important role for IMPα/β1 and IMPβ1 but not IMPβ2 for nuclear targeting. By combining quantitative confocal laser scanning

microscopy (CLSM) with biochemical and crystallographic assays, we could further show that specific NLSs selectively bind different IMPs and differently contribute to Pre-pVII subcellular localization. Indeed, NLSd (PP**RKRRR**VA-149) binds with high affinity to IMPα2, in analogous fashion to several cNLSs, whereas NLSa (GYW**RRKRS**K**K**A-53) preferentially binds to IMPβ1. On the other hand, NLSc (G**RK**I**KK**A**R**AP-120) is crucial in mediating nucleolar targeting/retention and can, therefore, be considered a nucleolar localization sequence (NoLS), whereas NLSb plays a minor but significant role by contributing to nucleolar and nuclear targeting.

2 | Materials and Methods

2.1 | Phylogenetic Analysis

Phylogenetic analysis based on adenovirus pVII was performed to determine the evolutionary affiliation of the genus *Siadenovirus* with the protein of interest. The amino acid sequences of pVII available in GenBank for genus *Siadenovirus* members were extracted and aligned with MAFTT (version 7.450), using Geneious (version 22.1.1; Biomatters Ltd, Auckland, New Zealand), using the following settings: scoring matrix BLOSUM62; gap open penalty 1.53; offset value 0.123. Following the amino acids sequence alignments, maximum likelihood (ML)-based phylogenetic analysis was performed with 500 nonparametric bootstrap replicates implemented in Geneious (version 22.1.1; Biomatters Ltd, Auckland, New Zealand).

2.2 | Identification of Putative NLSs on pVII

The primary sequence from FrAdV1 Pre-pVII (GenBank accession no: NC_002501) [1] was analyzed with the cNLS mapper software [29] and by visual inspection to identify putative NLSs.

2.3 | Tertiary Structure Prediction

AlphaFold2 [30] was utilized to predict a model for pVII in response to the absence of structural information. A comprehensive model for the full-length pVII of FrAdV1 [1] was created, emphasizing the identified NLS regions. In addition, for the purpose of structural comparison, we employed AlphaFold2 and generated a structural model for HAdV2 Pre-pVII [10].

2.4 | Plasmids

Bacterial expression plasmids mediating the expression of truncated version of mouse (m)IMPα2 lacking the autoinhibitory IMPβ1 binding (IBB) domain, and mIMPβ1 from a pET30a backbone were described previously [31, 32]. Mammalian expression plasmids pcDNA3.1-NT-GFP-TOPO and pcDNA3.1-NT-GFP-TOPO-SV40-LTA-NLS, mediating the expression of GFP cycle3, or of a fusion protein between GFP cycle3 and Simian vacuolating virus (SV) 40 large tumor antigen (LTA) NLS (PKKKRKV-132), respectively, were described previously [33]. Plasmid pEPI-GFP-UL44, encoding a fusion protein between GFP and human cytomegalovirus (HCMV) DNA polymerase UL44, localizing to the nucleus via the IMPα/β1 dependent pathway, was also previously described [34]. Plasmid pEGFP-C1-UL44(409-433), was synthesized by BioFab Research (Rome, Italy). Plasmid GST-GFP-FUS, encoding a fusion protein translocated in the nucleus via IMPβ2 [35], was kindly provided from Dorothee Dormann (Mainz, Germany), whereas plasmid pDsRed-C1-Fibrillarin [36] was kindly provided by Denis Archambault (University of Québec, Canada). Plasmid RFP-M9M, encoding a potent and selective IMPβ2 inhibitor [37] was provided by Yoshihiro Kino (Tokyo, Japan). Plasmid mCherry-Bimax2, encoding a competitive inhibitor of the IMPα/β1 nuclear import pathway, [38] was a generous gift from Yoshihiro Yoneda and Masahiro Oka (Osaka, Japan). Mammalian expression plasmids encoding GFP-FrAdV1 Pre-pVII (1-149) and substitution derivatives thereof, as well as GFP fused to FrAdV1 Pre-pVII individual NLS sequences, were synthesized by BioFab research (Rome, Italy) and GeneScript (New Jersey, USA). Plasmid pHM830 [39], encoding a fusion protein between GFP and β-galactosidase (β-Gal), was kindly provided by Thomas Stamminger (Ulm University Medical Center, Germany). Plasmid pHM830-SV40-LTA NLS, allowing the expression of the SV40 LTA NLS within GFP and β-gal, was previously described [40]. pHM830-FrAdV1, mediating the expression of FrAdV1 Pre-pVII fused between GFP and β-gal, as well as pHM830-FrAdV1-NLSa, pHM830-FrAdV1-NLSb, pHM830-FrAdV1-NLSc, and pHM830-FrAdV1-NLSd were synthesized by GeneScript (New Jersey, USA). A list of all plasmids used in this study is available in Table S1.

2.5 | Peptides

Synthetic peptides representing the predicted amino acid residues, with an *N*-terminal FITC tag, were synthesized by GenScript (Table S2).

2.6 | Expression and Purification of Recombinant Proteins

The overexpression of IMPs was carried out in *Escherichia coli* pLysS BL21(DE3) as described previously [41] using the autoinduction method [42]. After induction, the cultures were centrifuged at 6000 rpm for 20 min at 4°C, and the resulting bacterial pellets were resuspended in HIS buffer A (pH 8), which consisted of 50 mM phosphate buffer, 300 mM NaCl, and 20 mM imidazole. To lyse the cells, two freeze–thaw cycles were performed, followed by the addition of lysozyme (1 mL of 20 mg/mL) (Sigma-Aldrich, St. Louis, MI, USA) and DNase (10 μL of 50 mg/mL) (Sigma-Aldrich, St. Louis, MI, USA), and incubation at room temperature (RT) for 1 h. The supernatants containing soluble proteins were collected by centrifugation at 12000 rpm for 30 min at 4°C. The extracts were then filtered through 0.45 μm low protein affinity filters and injected into a 5 mL HisTrap HP column (GE Healthcare, Chicago, IL, USA) that had been pre-equilibrated with His buffer A, in an AKTA purifier FPLC system (GE Healthcare, USA). Followed by washes of 20 column volumes with His buffer A, the proteins of interest were eluted using a gradually increasing gradient of imidazole (ranging from 20 to 500 mM)

(ChemSupply, Gillman, SA, Australia). The eluted protein fractions were combined and loaded onto a pre-equilibrated HiLoad 26/60 Superdex 200 column (GE Healthcare, USA) in GST buffer A (50 mM Tris and 125 mM NaCl) for further purification using size-exclusion chromatography. The fractions corresponding to the eluted volumes at the respective protein sizes were collected, and the samples were concentrated using an Amicon MWCO 10 kDa filter (Merck Millipore, Burlington, MA, USA). Prior to experimental use, the purity of the samples was assessed by performing SDS-PAGE at 165 V for 30 min on a 4%–12% Bis-Tris Plus gel (Thermo Fisher Scientific, Waltham, MA, USA).

2.7 | Fluorescence Polarization (FP) Assays

FITC-tagged FrAdV1 Pre-pVII NLS peptides (Table S2) at a concentration of 2 nM were incubated with mIMPα2ΔIBB and IMPβ1 in twofold serial dilutions, starting from 20 μM, across 23 wells to a final volume of 200 μL per well in GST buffer A (50 mM Tris, 125 mM NaCl), with the last well not containing any IMPs, essentially as described previously [43, 44]. FP measurements were conducted using a CLARIOstar Plus plate reader (BMG Labtech, Germany) in 96-well black Fluotrac microplates (Greiner Bio-One, Austria). Assays were carried out in three independent experiments, each including an appropriate negative control (no IMP binding partner). Data were analyzed with GraphPad Prism (Prism 9, Version 9.3.1), and a binding curve was fitted to determine the dissociation constant (K_d) and maximum binding (B_{max}). A summary of the FP assay results is presented in Table S3.

2.8 | Crystallization, Data Collection, and Structure Determination

The hanging drop vapor diffusion method was employed to crystallize the IMPα2ΔIBB:FrAdV1 Pre-pVII NLS protein complex. The complex was attained in a 1:1 M ratio, with each hanging drop having a total volume of 3 μL over a well of 300 μL precipitant solution containing 650 mM sodium citrate (pH 6.5) and 10 mM DTT at a temperature of 23°C. Crystals were formed after 3 days of incubation. Formed crystals were collected and cryoprotected in a precipitant solution containing 20% glycerol, before being rapidly frozen in liquid nitrogen. X-ray diffraction data were obtained at the Australian Synchrotron using the MX2 macromolecular beam line, utilizing an Eiger 16M detector [45]. The data obtained were subjected to indexing and integration using XDS [46]. Subsequent steps including merging, space group assignment, scaling, and Rfree calculations were carried out using AIMLESS within CCP4, a suite of programs for crystallographic data processing [47]. The final model building and refinement were performed using software tools that are commonly used for model building and refinement in structural biology, COOT [48], and Phenix [49]. Phasing was performed using molecular replacement in Phaser [50] and PDB code 3UKX was used as the search model for IMPα2. The finalized model was subjected to validation and subsequently deposited to the Protein Data Bank (PDB) with an assigned accession number 8U36; refinement statics are detailed in Table S4. The binding interactions were calculated using PDBePISA [51].

2.9 | Cells

HEK293A cells were maintained in Dulbecco's modified Eagle's medium (DMEM) supplemented with 10% (v/v) fetal bovine serum (FBS), 50 U/mL penicillin, 50 U/mL streptomycin, and 2 mM L-glutamine in a humidified incubator at 37°C in the presence of 5% CO_2 and passaged when reached confluence as described in the work of Messa et al. [52].

2.10 | Transfections

HEK293A cells were seeded in a 24-well plate onto glass coverslips (5×10^4 cells/well). The next day, cells were transfected with appropriate amounts of expression constructs (range 5–250 ng), using Lipofectamine 2000 (ThermoFisher Scientific, Monza, Italy), following the manufacturer's recommendations and further incubated at 37°C and 5% CO_2 in complete medium as described [53], until being processed for CLSM.

2.11 | CLSM and Image Analysis

Cells were transfected and incubated for 24 hour to allow expression of spontaneously fluorescent proteins. Afterward, the cells were treated with DRAQ5 (#62251; ThermoFisher Scientific, Monza, Italy) at a dilution of 1:5000 in DMEM without phenol red for 30 min [54]. Following incubation, the cells were washed twice with PHEM 1× solution (60 mM PIPES, 25 mM HEPES, 10 mM EGTA, and 4 mM $MgSO_4$) and fixed with 4% paraformaldehyde (v/v) for 10 min at RT. After three washes with PBS 1×, coverslips were mounted on glass slides using Fluoromount G (Southern Biotech, Birmingham, AL, USA). The subcellular localization of fusion proteins was examined using a Nikon A1 confocal laser scanning microscope (Nikon, Tokyo, Japan) equipped with a 60× oil immersion objective, following the established protocol outlined in the studies by Alvisi et al. and Smith et al. [55, 56] to determine the levels of nuclear accumulation of the proteins of interest, the FiJi public domain software (https://doi.org/10.1038/nmeth.2019) was utilized, and single-cell measurements were taken for nuclear (Fn), nucleolar (Fno), and cytoplasmic (Fc) fluorescence. DRAQ5 and fibrillarin were used to define nuclear and nucleolar masks, respectively, whereas a small area close to DRAQ5 was used to define a cytosolic mask as previously [28]. The fluorescence attributed to autofluorescence/background (Fb) was subtracted from the measurements to calculate the Fn/c and Fno/Fn ratios according to the formulas $Fn/c = (Fn - Fb)/(Fc - Fb)$ and $Fno/Fn = (Fno - Fb)/(Fn - Fb)$. Cells with oversaturated signals were excluded from analysis. In some cases, to allow easier detection of nucleoli, cells were co-transfected with a DsRed-fibrillarin expression plasmid, and rgb profile plots were calculated with FiJi. Statistical analysis was performed using GraphPad Prism 9 software (GraphPad, San Diego, CA, USA) applying Student's *t*-test, one-way ANOVA, or two-way ANOVA, as appropriate.

2.12 | Inhibition of Ran-Dependent Nuclear Transport

Ran-dependent nuclear transport was inhibited by depletion of cellular RanGTP resulting from a lack of free GTP [57], by incubating cells for 30 min at 37°C in DMEM containing no glucose, 5% FBS, and supplemented with 10 mmol/L sodium azide, 6 mmol/L 2-deoxy-D-glucose (D8357, Sigma, Merck Millipore, Milan, Italy) and DRAQ5 (#62251; ThermoFisher Scientific, Monza, Italy; 1:5000) as described in the work by Alvisi et al. [58], before being fixed and analyzed by CLSM as detailed above.

3 | Results

3.1 | Evolution of Pre-pVII in Siadenoviruses and Identification of NLSs Within Frog Siadenovirus 1 (FrAdV1)

Nuclear transport of AdV pVII has been partially characterized for HAdV [8, 10, 12]. Several studies reported that HAdVs pVII utilize several different NLSs, enabling transportation to the host cell nucleus via various import pathways, whereas very little is known for other AdVs [13, 28]. Although HAdV2 Pre-pVII localized to the nucleolus, we have recently shown that the psittacine siadenovirus F (PsSiAdV) Pre-pVII mainly localized in the nucleoplasm, when expressed in the absence of any other viral proteins, implying important differences in nuclear localization among diverse AdVs [28]. To gain insights into the evolutionary aspects of pVII among siadenovirus members, we performed a phylogenetic analysis using their primary amino acids sequences and identified FrAdV1 pVII as the most ancient form within the genus *Siadenovirus* (Figure 1A). To better understand the nuclear transport of FrAdV1 Pre-pVII, we analyzed its primary sequence bioinformatically with cNLS mapper and by visual inspection for putative NLSs. Such analysis revealed four putative NLSs (NLSa: $_{43}$GYW**RRKRS**K**K**A$_{53}$, NLSb: $_{74}$**RKK**IP**K**TPVGVVGPLWQGT**RKR**$_{95}$; NLSc: $_{111}$G**RK**I**KK**A**R**AP$_{120}$, and NLSd: $_{141}$PP**RKRRR**VA$_{149}$), of which NLSb was identified a putative bipartite NLS (Figure 1B,C). FrAdV1 and HAdV2 Pre-pVII share very little sequence identity (26.1%). Accordingly, the identified NLSs have no clear counterparts in HAdV2 Pre-pVII (Figure 1B,C).

Since the structure of Pre-pVII proteins is yet to be determined, we employed AlphaFold2 to generate models that may provide preliminary insights into their structure (Figure S1). Predictions suggested HAdV2 Pre-pVII to be disordered, with an unstructured N-terminus (comprised of a loose string of five alpha helices, and two beta strands separated by flexible loops) and a disordered C-terminus (Figure S1A–C). AlphaFold2 also predicted FrAdV1 Pre-pVII to be an intrinsically disordered protein with no structured regions (Figure S1D,E). It is worth noting that AlphaFold2 may have difficulty predicting the structure of proteins with large, disordered regions or for proteins where experimental data have not previously been obtained. Therefore, it is possible that FrAdV1 Pre-pVII does contain structured regions not depicted in the AlphaFold prediction. However, the prediction of FrAdV1 Pre-pVII to be disordered suggests that it may be flexible and dynamic, able to adopt multiple conformations, and therefore accessible for binding to nuclear import receptors.

3.2 | FrAdV1 Pre-pVII Protein Strongly Accumulates in the Nucleolus in the Absence of Other Viral Proteins

To investigate the subcellular localization of FrAdV1 Pre-pVII, we transiently expressed in mammalian cells a Pre-pVII GFP-fusion protein and compared its subcellular localization to similar fusions with HAdV2 Pre-pVII and PsSiAdV Pre-pVII, which are known to accumulate into the nucleoli and nucleoplasm, respectively [28]. As further controls, GFP alone and GFP fused to human cytomegalovirus (HCMV) DNA polymerase processivity factor UL44 were also expressed [40], whereas DsRed-fibrillarin was used as a marker for nucleolar localization (Figure 2A). As expected, GFP alone localized with a diffuse pattern distributed between the nuclei and cytoplasm, whereas UL44 strongly accumulated in the cell nucleus, and both proteins were largely excluded from the nucleoli (Figure 2B). As recently shown, Pre-pVII from PsSiAdV exhibited a localization reminiscent of UL44, while HAdV2 accumulated in the nucleoli and colocalized with fibrillarin, although a considerable fraction of the protein was detectable in the nucleoplasm (Figure 2B). Intriguingly, FrAdV1 Pre-pVII strongly accumulated in the nucleoli, with limited detection in the nucleoplasm, displaying a different localization pattern to its HAdV2 and PsSiAdV orthologs (Figure 2B).

3.3 | FrAdV1 Pre-pVII NLSs Can Bind to Different Cellular Transporters

Given their ability to interact with multiple IMPs, HAdVs pVIIs are believed to be transported into the nucleus by multiple pathways [10]. We therefore assessed the binding of each FrAdV-1 putative NLS to bind to mIMPα2ΔIBB and IMPβ1 using a quantitative FP assay (Figure 3 and Table S3), commonly used in the field [28, 31, 33, 43, 44]. Interestingly, NLSa interacted with IMPβ1 with high affinity (B_{max} = 140.6 mP units; K_d = 17.2 nM), whereas NLSd showed high affinity for mIMPα2ΔIBB (B_{max} = 216.2 mP units; K_d = 49.3 nM). On the other hand, NLSb and NLSc bound with low affinity to both mIMPα2ΔIBB and IMPβ1 (Figure 3 and Table S3). These results suggest that FrAdV1 Pre-pVII can interact with different IMPs via distinct NLSs, being therefore transported into the nucleus via several pathways.

3.4 | FrAdV1 Pre-pVII NLSs Can Confer IMPα/β1 Dependent and Independent Nuclear Import to Heterologous Proteins

Since the FrAdV1 Pre-pVII strongly accumulated in the nucleoli of transfected cells and contains four putative NLSs (Figure 2B,C) that can mediate binding to several IMPs (Figure 3), we analyzed the ability of such NLSs to alter the subcellular localization of a reporter protein. To this end, we analyzed the subcellular localization of fusion proteins between GFP and FrAdV1 Pre-VII putative NLSs when transiently

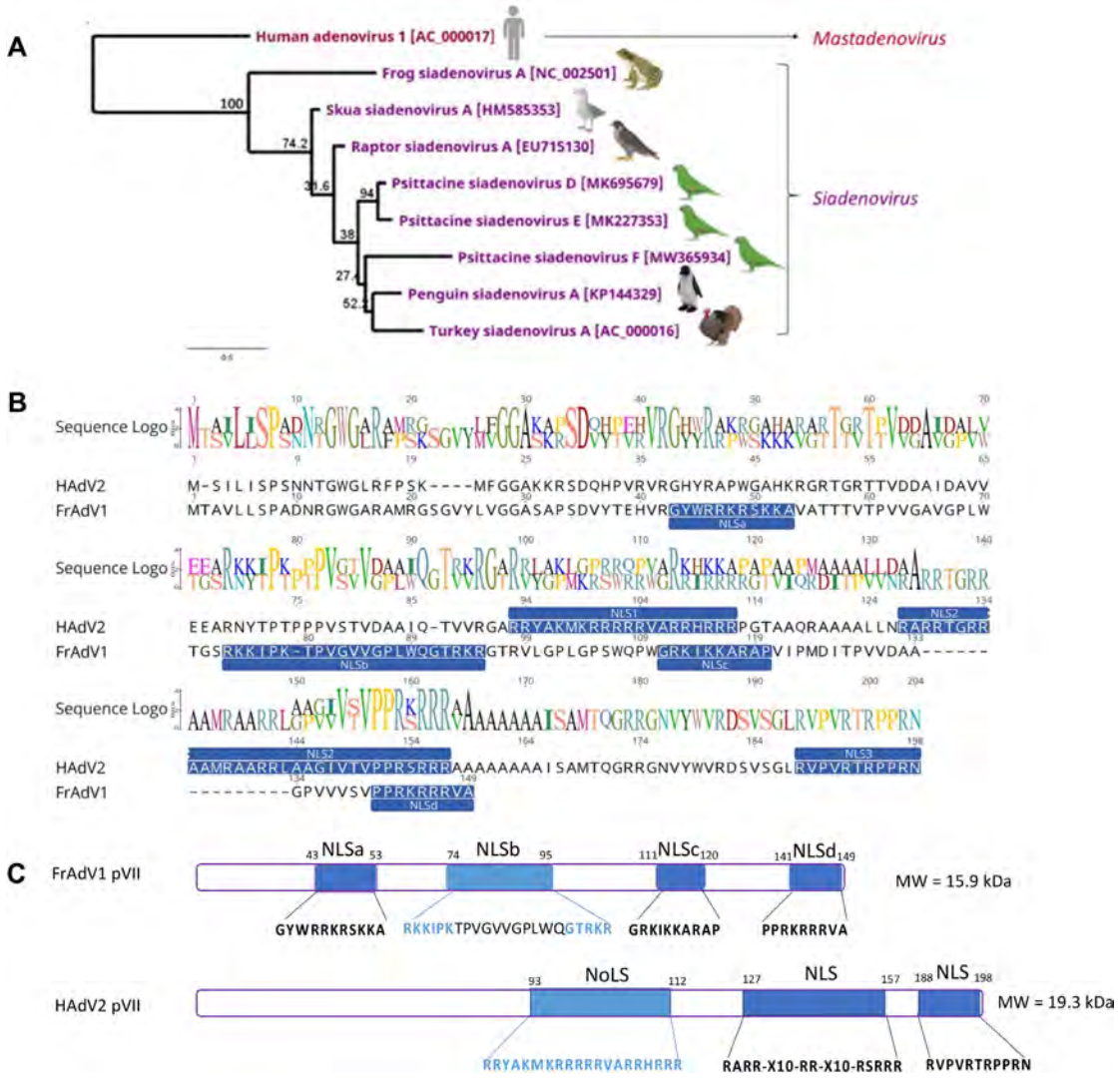

FIGURE 1 | The evolution of pVII in siadenoviruses and identified NLSs in FrAdV1 pVII. (A) The phylogenetic tree exhibits the possible evolutionary relationship of siadenoviruses based on protein VII. The numbers on the left show bootstrap values as percentages, and the labels at branch tips refer to adenovirus species name, followed by GenBank accession number in parentheses. (B) pVII sequences from FrAdV1 (GenBank Accession no: NC_002501) [7] and HAdV2 (GenBank Accession no: AC_000008) were aligned using Geneious Prime. Previously described NLSs and NoLS are highlighted in dark and light blue shadings, respectively. (C) Simplified diagram displaying the identified putative NLS regions of FrAdV1 pVII and previously described NLSs and NoLS from HAdV2 [7, 8, 10].

expressed in mammalian cells (Figure 4A), followed by quantitative analysis on nuclear and nucleolar accumulation levels (Figure 4B,C). We also expressed GFP alone and GFP fused to SV40 LTA NLS, as negative and positive controls for nuclear accumulation, respectively. As expected, GFP alone equally distributed between nucleus and cytoplasm (Figure 4B) with a Fn/c of 1.2 (Figure 4C), whereas GFP-SV40 LTA NLS strongly accumulated in the cell nucleus (Figure 4B), with a Fn/c of 6.9 (Figure 4C). Both proteins were partially excluded from the nucleoli with a Fno/Fn < 1 (Figure 4D). Importantly, fusion to each FrAdV1 Pre-pVII-NLS affected GFP subcellular localization, although to different extents. The highest levels of nuclear accumulation were observed for GFP-FrAdV1 pVII-NLSd, with a Fn/c of 7.2 (Figure 4C), and similarly to GFP alone, it was mainly excluded from nucleoli (Fno/n < 1, Figure 4D). On the other hand, while nuclear accumulation mediated by either NLSa or NLSc was considerably lower as compared to NLSd, both sequences could significantly increase GFP targeting to the nucleolus (Figure 4D). Finally, NLSb slightly increased GFP nuclear targeting (Fn/c of c. 2, see Figure 4C), but not its nucleolar accumulation (Fno/n < 1, see Figure 4D). Our results suggest that FrAdV1 Pre-pVII contains four sequences which could contribute to its nuclear localization (NLSa-d), and two (NLSa and NLSc) which could contribute to its nucleolar targeting. Since we and others have extensively shown that the peptide inhibitor Bimax2 can abolish IMPα/β1-dependent nuclear import [29, 33, 58], we decided to test its effect on the activity of FrAdV1 Pre-pVII NLSs. We therefore tested the effect of co-expression with mCherry-Bimax2 on the nuclear accumulation of the FrAdV1 Pre-pVII NLSs GFP fusion proteins (Figure S2). As expected, expression with Bimax2 completely abolished nuclear targeting of GFP-SV40 LTA NLS (Figure S2), consistent with its ability to bind exclusively to IMPα/β1 via IMPα. Importantly, Bimax2 significantly reduced nuclear accumulation mediated by NLSd but not by NLSa, NLSb, and NLSc (Figure S2B). These results are consistent with FrAdV1 Pre-pVII NLSd being a cNLS

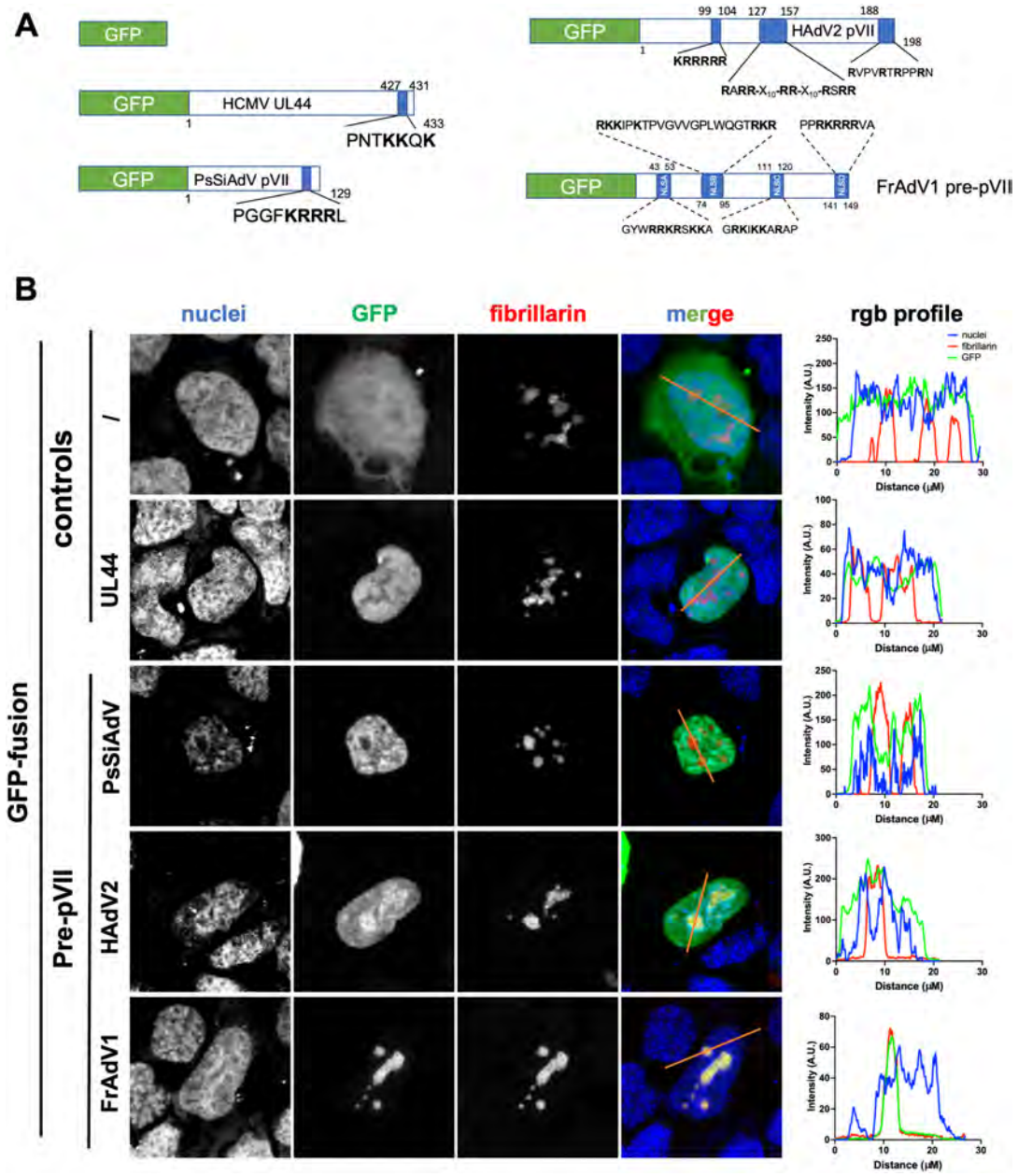

FIGURE 2 | FrAdV1 Pre-pVII proteins localizes to the cell nucleus and accumulates in the nucleoli. (A) Schematic representation of the GFP-fusion proteins expressed. Proteins are represented by *white horizontal bars*. NLSs are shown as *blue vertical bars*, along with their amino acidic sequence. The *single letter* amino acid code is used. Basic residues are in *boldface*. (B) The indicated GFP fusion proteins were transiently co-expressed in HEK293A with DsRed-fibrillarin by means of Lipofectamine 2000 transfection. Twenty-four-hour post transfection, cells were incubated with DRAQ5 to stain cell nuclei, fixed with paraformaldehyde and processed for CLSM analysis as described in the Materials and Methods section. Representative images of the 633 nm (*nuclei*), 488 nm (*GFP*), and 561 nm (*fibrillarin*) laser channels are shown, along with a merged image (*merge*), and a rgb profile plot across the indicated area (*rgb profile*).

functionally interacting with IMPα. Since the GFP-NLS fusion protein tested can passively diffuse in the nucleus due to their limited molecular weight, the activity of FrAdV1 putative NLSs was further assessed by comparing their ability to translocate into the nucleus the otherwise cytoplasmic GFP-β-gal reporter protein, whose molecular weight is well-above that sufficient to allow efficient passive diffusion across the NPC [39]. As a positive control, the subcellular localization of GFP-β-gal fused to SV40 LTA NLS was also assessed (Figure S3A). As expected, GFP-β-gal localized mainly in the cytoplasm (Fn/c of 0.4, see Figure S3B,C), while fusion to SV40 LTA NLS resulted in a strong nuclear localization (Fn/c of 27.1, see Figure S3B,C). Among FrAdV1 Pre-pVII NLSs, only NLSd targeted GFP-β-gal to the nucleus (Fn/c 23.6), while no effect on nuclear localization was observed after fusion of other NLSs (Figure S3B,C). Importantly, co-expression with Bimax2 significantly impaired nuclear translocation of GFP-β-gal when fused to either SV40 LTA NLS (Fn/c 2.5) or FrAdV1 NLSd (Fn/c 1.9). These results suggest that, when placed outside of their physiological location, only NLSd can confer active nuclear targeting to a reporter

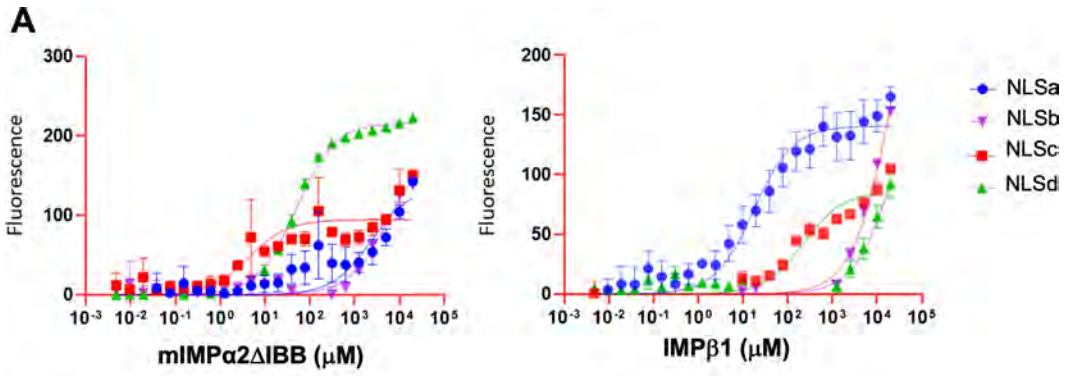

B

FITC-labelled peptide	*Kd* ± SD (nM)	
	mIMPα2ΔIBB	IMPβ1
NLSa	2333 ± 788	17 ± 4
NLSb	5236 ± 936	20 407 ± 5774
NLSc	4 ± 1	227 ± 68
NLSd	49 ± 2	22 776 ± 10 624

FIGURE 3 | FP analysis of FrAdV1 Pre-pVII NLS peptides interaction with IMPs. Synthetic FITC tagged FrAdV1 Pre-pVII NLS peptides (2 nM) were incubated with twofold serially diluted mIMPα2ΔIBB (left) and IMPβ1 (right), starting from 20 μM, across 23 wells to a final volume of 200 μL per well in GST buffer A (50 mM Tris, 125 mM NaCl). (A) Data are shown as mean ± standard error of the mean (SEM) relative to three independent experiments. Data were analyzed with Graphpad Prism using the one site-specific binding least squares fit function to calculate the B_{max} and K_d relative to the peptide:IMPα2ΔIBBs interaction. (B) A summary table relative to data shown in (A), with mean K_d values relative to the interaction of indicated peptides with IMPs, along with the respective standard deviation of the mean (SD).

protein which cannot passively diffuse across the NPC, in an IMPα/β1-dependent fashion.

3.5 | High-Resolution Crystal Structure Uncovers the Classical Binding Interface of IMPα FrAdV1 Pre-pVII NLSd

Based on our observation that the FrAdV1 Pre-pVII NLSd bound with high affinity to IMPα2, we undertook x-ray crystallography of this complex to gain a deeper understanding of the interactions between FrAdV1 Pre-pVII and host cellular transporters, and the data were indexed in P212121, with unit cell parameters of $a = 77.29$, $b = 89.29$, and $c = 95.80$. The resolved structure identified one chain of FrAdV1 Pre-pVII NLSd (PP**RKRRR**VA-149) bound to mIMPα2ΔIBB (Figure 5A), with NLSd residues 143–147 accommodated in the IMPα2 P1-P5 binding sites (Figure 5B). Furthermore, an additional interaction was observed outside the P1-P5 binding sites, between NLSd residue Ala^{149} and IMPα2 Ser^{105}. The well-characterized and thermodynamically dominant IMPα2 P2 site (comprised of Gly150, Thr155, and Asp192) is occupied by NLSd Lys144, which can be therefore considered the predominant determinant of binding. Accordingly, NLSd Lys144 forms two hydrogen bonds with IMPα2 residues Gly150 and Thr155, and a salt bridge with Asp192 (Figure 5B,C). NLSd Arg143 binds to IMPα2 P1 binding site Asp270 via a salt bridge. NLSd Arg145 interacts with the P3 binding site of IMPα2 at Asn188 and Asn288, via hydrogen bonding, whereas NLSd Arg146 interacts with P4 residues Leu104 and Arg106. Finally, NLSd Arg147 interacts with P5 IMPα2 residues Asn146 and Gln181 (Figure 5C). Furthermore, when an excessive amount of peptide was employed, NLSd was found at IMPα2 minor binding site (not shown). Our results are therefore consistent with NLSd being a cNLS functionally interacting with IMPα2 major binding site and K144 being the key residue involved in the interaction.

3.6 | FrAdV1 Pre-pVII Can Accumulate in the Nucleolus by Multiple Nuclear Import Pathways

Since nuclear import of HAdV2 Pre-pVII and mature pVII has been shown to rely on IMPα/β1 and IMPβ2, respectively [10], we analyzed the effect of inhibitors of the IMPα/β1 and IMPβ2 nuclear import pathways on the subcellular localization of FrAdV1 Pre-pVII. Inhibitors tested include mCherry-Bimax2 [38], which impairs IMPα/β1-dependent nuclear import and M9M-RFP [37], which inhibits IMPβ2-dependent nuclear import (Figure 6A). GFP-UL44, which is imported into the nucleus by IMPα/β1, was also expressed as a control [40]. As previously, in the absence of nuclear import inhibitors, both GFP-UL44 and FrAdV1 Pre-pVII strongly localized to the cell nucleus (Figure 6B and Figure S4), with a Fn/c > 10 (Figure 6C). Co-expression with mCherry-Bimax2 (Fn/c 0.3) strongly impaired nuclear accumulation of GFP-UL44, while no significant reduction was observed in the presence of RFP-M9M (Figure 6C). Surprisingly, GFP-FrAdV1 Pre-pVII nuclear import was not significantly impaired by any inhibitor tested. The lack of response to either Bimax2 or M9M can be interpreted as the consequence of the ability of Pre-pVII to simultaneously

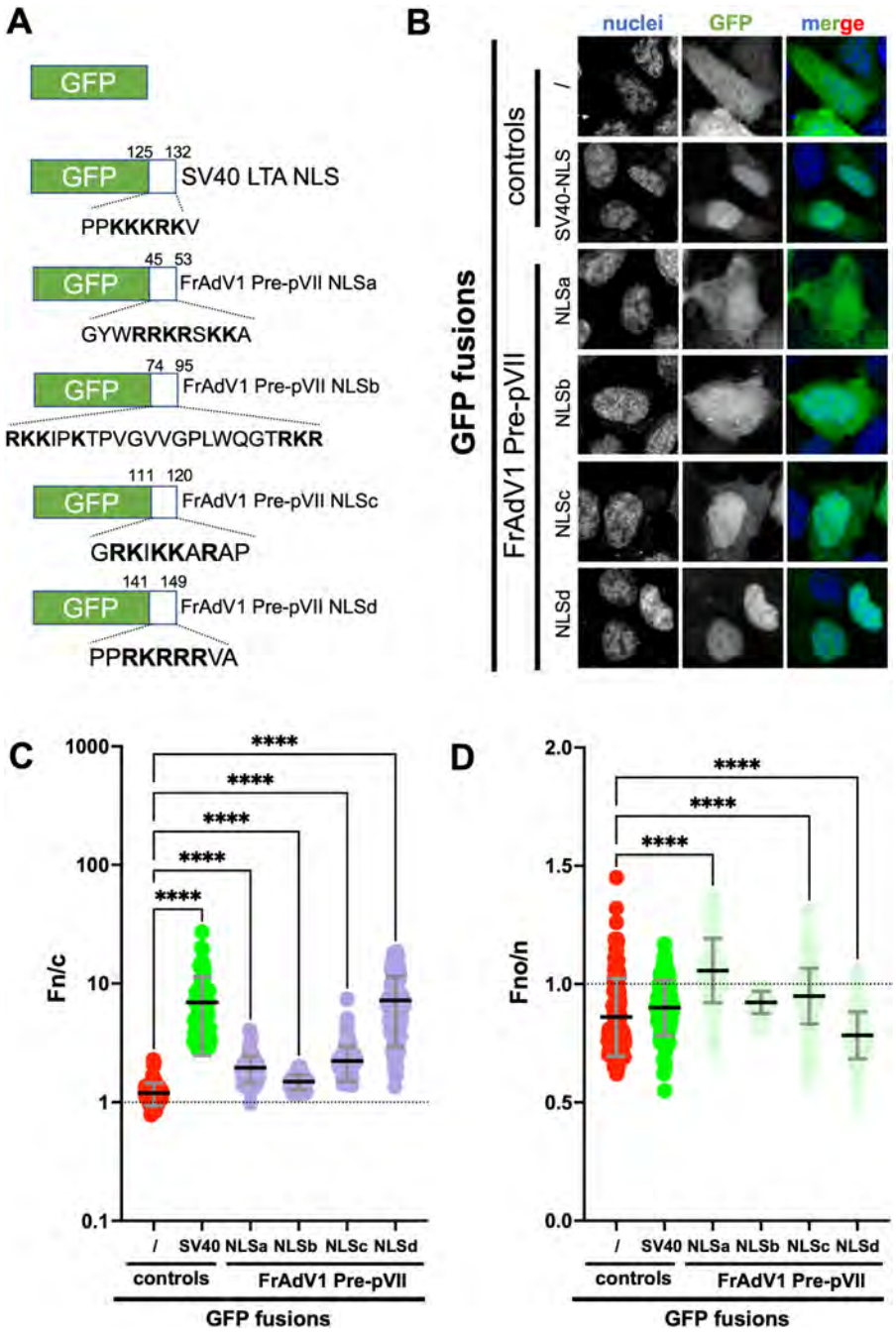

FIGURE 4 | FrAdV1 Pre-pVII contains multiple functional NLSs. (A) Schematic representation of the GFP-fusion proteins expressed, with NLSs represented as white boxes, along with their amino acid sequence and position. (B) HEK293A cells were seeded on glass coverslips and transfected to express the indicated GFP fusion proteins. Twenty-four-hour post transfection cells were incubated with DRAQ5 to stain cell nuclei, fixed and coverslips mounted on slide holders before being analyzed by using a Nikon A1 CLSM equipped with a 60× oil immersion objective. Representative images of the 633 nm (*nuclei*), and 488 nm (GFP) laser channels are shown, along with a merged image (*merge*). Micrographs such as those shown were used for image analysis by measuring nucleolar (Fno), nuclear (Fn), cytoplasmic (Fc), and background (Fb) fluorescence for single cells using FiJi. (C) The levels of nuclear accumulation (Fn/c) were calculated using the formula Fn/c = (Fn − Fb)/(Fc − Fb). (D) The levels of nucleolar accumulation (Fno/n) were calculated using the formula Fno/n = (Fno − Fb)/(Fn − Fb). Data shown are individual measurements (*circles*), along with means (black horizontal bars) ± standard deviation (SD) of the mean relative to >45 cells from three independent experiments per each GFP fusion protein, along with the results of Welch and Brown–Forsythe ANOVA statistical analysis as compared to GFP alone (/). ****$p < 0.0001$.

interact with multiple IMPs. In addition to GFP-FrAdV1 Pre-pVII, which can passively diffuse into the nucleus due its molecular weight of c. 44 kDa, we also expressed a fusion between FrAdV1 Pre-pVII and the otherwise cytoplasmic GFP-β-gal reporter protein. Importantly, GFP-β-gal Pre-pVII accumulated in the nucleoli (Figure 6B) with a Fn/c > 2.8 (Figure 6C). This result clearly demonstrated that FrAdV1 Pre-pVII can be actively transported into the cell nucleus, despite its low molecular weight. Consistent with results obtained after fusion to GFP alone, neither mCherry-Bimax2 nor RFP-M9M could

significantly inhibit nuclear targeting (Figure 6C), further suggesting than Pre-pVII can be transported in the nucleus using multiple nuclear import pathways, thanks to the simultaneous presence of multiple NLSs interacting with different IMPs.

3.7 | Molecular Dissection of the Role of FrAdV1 Pre-pVII Individual NLSs in Nuclear and Nucleolar Targeting

To verify such hypothesis, we dissected the contribution of each NLS identified here to FrAdV1 Pre-VII nuclear and nucleolar targeting. Therefore, we quantitatively analyzed the subcellular localization of transiently expressed GFP fusion proteins with FrAdV1 Pre-pVII and several substitution derivatives thereof, whereby NLS basic residues were replaced either by A or T (Figure 7A), using DsRed-fibrillarin as a nucleolar marker. Importantly, individual inactivation of single NLSs did not significantly reduce nuclear accumulation (Figure 7B,C), with barely no signal being detectable in the cytosol of cells expressing GFP-FrAdV1 Pre-pVII wt (Fn/c of 15.5), mNLSa (Fn/c of 13.7), mNLSb (Fn/c of 13.9), mNLSc (Fn/c of 18.0), and mNLSd (Fn/c of 14.3). Simultaneous inactivation of either NLSa and NLSc (mNLSac, Fn/c of 11.5), NLSa and NLSd, (mNLSad, Fn/c of 11.3), or NLSc and NLSd (mNLScd, Fn/c of 14.8) only mildly reduced nuclear localization (Figure 7C). These results confirm that, when any of FrAdV1 Pre-VII NLS is individually inactivated, the others can functionally compensate for its absence. However, simultaneous inactivation of NLSa, NLSc, and NLSd was sufficient to significantly reduce nuclear accumulation (mNLSacd, Fn/c of 7.2). These data suggest that NLSb is functional in the context of full-length protein, but not sufficient to mediate optimal nuclear targeting. Accordingly, further inactivation of NLSb completely abolished nuclear accumulation (mNLSabcd, Fn/c 1.5). Therefore, FrAdV1 contains multiple functional NLSs responsible for its nuclear targeting.

On the other hand, almost any substitution introduced in FrAdV1 Pre-pVII NLSs significantly affected nucleolar accumulation, although to a different extent (Figure 7B). Quantitative analysis revealed that GFP-FrAdV1 Pre-pVII nucleolar accumulation (Fno/n of c. 14.3) was minimally affected by substitutions within NLSa (mNLSa, Fno/n of 11.8) or NLSd (mNLSd, Fno/n of 10.3), while it was clearly affected by substitution of either NLSb (mNLSb, Fno/n of 3.6) and especially NLSc (mNLSc, Fno/n of 1.3). Overall, all derivatives containing substitutions within NLSc failed to strongly accumulate in the nucleoli, confirming that NLSc ($_{111}$**G**R**KIKKA**R**A**P$_{120}$) has a major role in nucleolar accumulation, while NLSb ($_{74}$**RKK**IP**K**TPVGVVGPLWQGT**RKR**$_{95}$) also contributes to nucleolar targeting.

3.8 | FrAdV1 Pre-pVII Subcellular Localization Is the Result of Ran-Dependent Nuclear Import and Binding to Nucleolar Components, as Mediated by Specific NLSs

To more precisely characterize the contribution of each NLS identified in this study to the functional interaction with specific

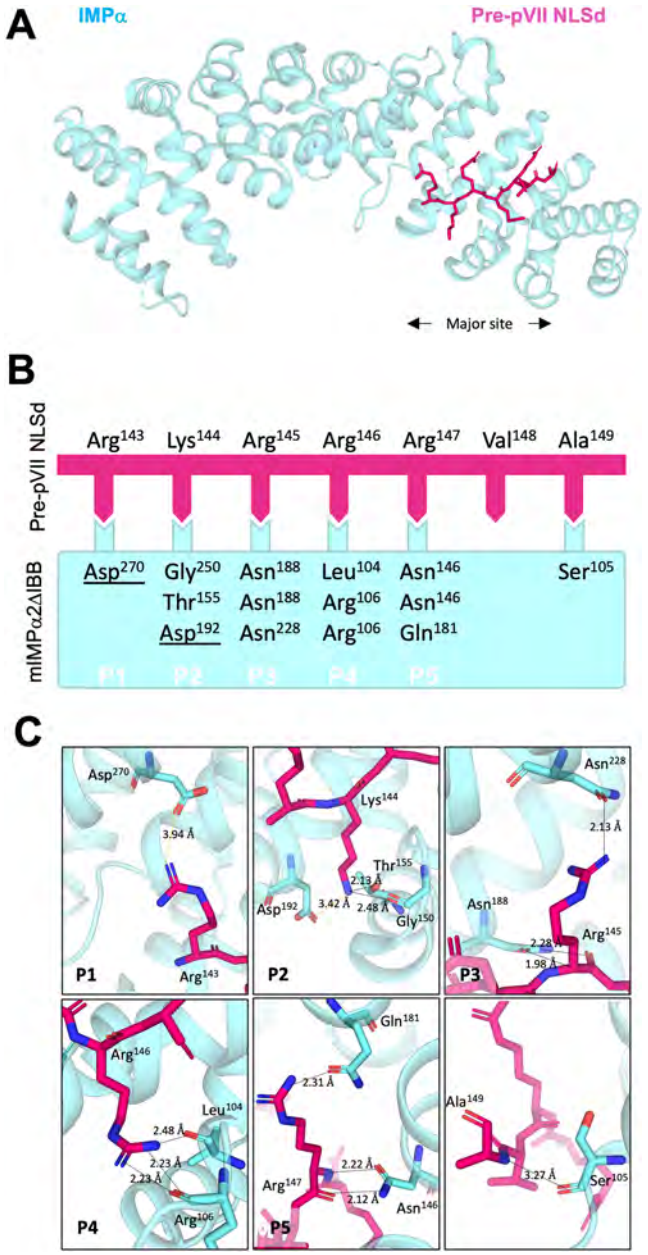

FIGURE 5 | Crystal structure of adenovirus FrAdV1 Pre-pVII NLSd bound to IMPα2ΔIBB. The structure of mIMPα2ΔIBB protein crystals in complex with FrAdV1 Pre-pVII NLSd FITC-labeled peptide was solved at 2.2Å resolution and visualized by Pymol. (A) FrAdV1 Pre-pVII NLSd is represented as magenta sticks bound to mIMPα2ΔIBB (cyan cartoon representation) at the major binding site. (B) Schematics representing the interface between FrAdV1 Pre-pVII NLSd (magenta) and mIMPα2ΔIBB major binding site (cyan). The P1-P5 binding sites are indicated, along with the interacting residues. IMPα2 residues forming salt bridges are underlined. (C) Close-up images of FrAdV1 Pre-pVII NLSd (magenta sticks) and IMPα2 (cyan sticks) major binding site interfacing residues, with interactions calculated by PDBePISA. Binding pockets P1-P5 are shown. Salt bridges are marked by dotted golden lines and hydrogen bonds with black dotted lines. Distances are in Angstrom (Å).

IMPs, we analyzed the effect of specific inhibitors nuclear import pathways on the subcellular localization of the FrAdV1 Pre-pVII substitution derivatives. To this end, mammalian cells

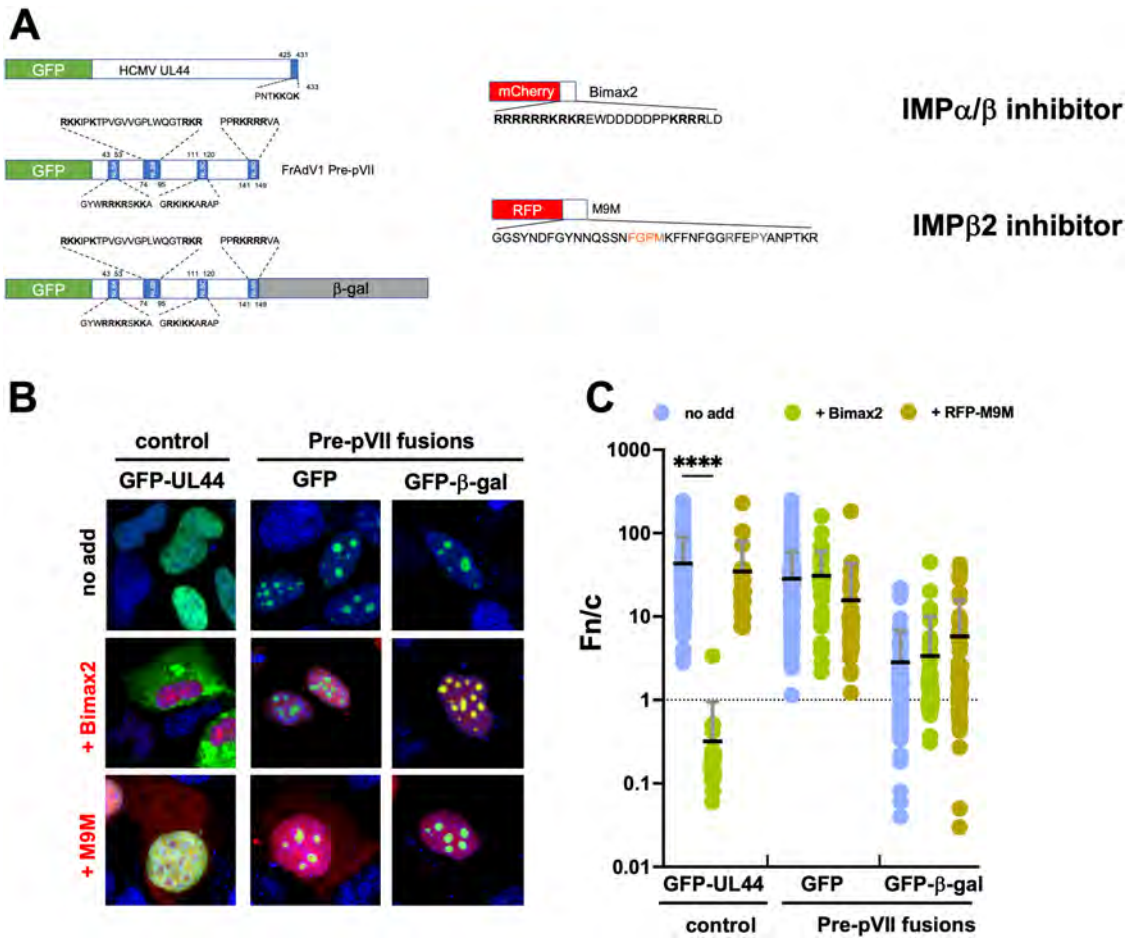

FIGURE 6 | FrAdV1 Pre-pVII proteins accumulates in the nucleoli independently of IMPα/β1 and transportin-1. **(**A) Schematic representation of GFP-FrAdV1 Pre-pVII. FrAdV1 Pre-pVII sequence is represented by a white horizontal bar. Putative cNLSs are shown as blue vertical bars, along with their amino acidic sequence. The single letter amino acid code is used. Basic residues are in boldface. (B) The indicated GFP fusion proteins were transiently expressed in HEK293A by means of Lipofectamine 2000 transfection, in the absence (*no add*) or in the presence of plasmids mediating the expression of either mCherry-Bimax2 (+ *Bimax2*) or RFP-M9M (+*M9M*). Twenty-four-hour post transfection cells were stained with DRAQ5 to stain cell nuclei, fixed with paraformaldehyde and processed for CLSM analysis as described in the Materials and Methods section. Representative merged images of cell nuclei (*blue*), GFP fusion proteins (*green*), and mCherry-Bimax2/RFP-M9M (*red*) are shown. (C) Micrographs such as those shown in (B) were quantitatively analyzed to calculate the levels of nuclear accumulation (Fn/c) relative to the indicated fusion proteins at the single cell level, as described in the Materials and Methods section. Data shown are individual measurements (*circles*), along with means (*black horizontal bars*) ± standard deviation of the mean (SD) relative to pooled data from at least 27 cells from two independent experiments. Results from two-way ANOVA test for the nuclear accumulation of the indicated GFP-fusion proteins in the absence or in the presence of M9M or Bimax2 are shown. ****$p < 0.0001$.

were transfected to express GFP-fusion proteins (Figure 8A) in the presence and absence of mCherry-Bimax2, or RFP-M9M, and microscopic images were captured by CLSM (Figure 8B and Figure S6–S12), followed by quantitative analysis of the levels of nuclear (Figure 8C) and nucleolar (Figure 8D) accumulation. To test the dependency of Ran-dependent nuclear import, we also depleted intracellular GTP by incubating cells in the presence of sodium azide and 2-dexoxy-D-glucose [57]. As expected, depletion of intracellular GTP strongly inhibited nuclear accumulation of GFP-UL44(409–433), a fusion protein which contains UL44-NLS fused to GFP and is actively transported into the nucleus by the IMPα/β1 heterodimer, but sufficiently small to passively diffuse across the NPC (Figure S5A,B), but not that of GFP-UL44, which is too large to diffuse out of the nucleus after inactivation of Ran-dependent nuclear import (Figure 8B,C). Importantly, depletion of intracellular GTP did not affect the nuclear accumulation of GFP-FrAdV1 Pre-pVII (Figure 8B,C). Since GFP-FrAdV1 Pre-pVII is sufficiently small to passively diffuse across the NPC once Ran-dependent nuclear import is inhibited, this result strongly suggests its ability to bind to intranuclear components after active nuclear import. Accordingly, depletion of intracellular GTP significantly inhibited nuclear import of all GFP-FrAdV1 Pre-pVII substitution derivatives lacking NLSc which are impaired in nucleolar targeting (mNLSc, mNLSac, mNLScd, and mNLSabc; see Figure 8B,C and Figures S7). This suggests that Pre-pVII is capable of binding to nucleolar components dependent on NLSc, which functions as an NoLS. In the absence of such NoLS, the protein can diffuse out of the nucleus upon inhibition of Ran-dependent active nuclear import. Intriguingly, nuclear accumulation of FrAdV1 Pre-pVII derivatives was not affected by Bimax2 co-expression, unless both NLSa and NLSc were simultaneously inactivated,

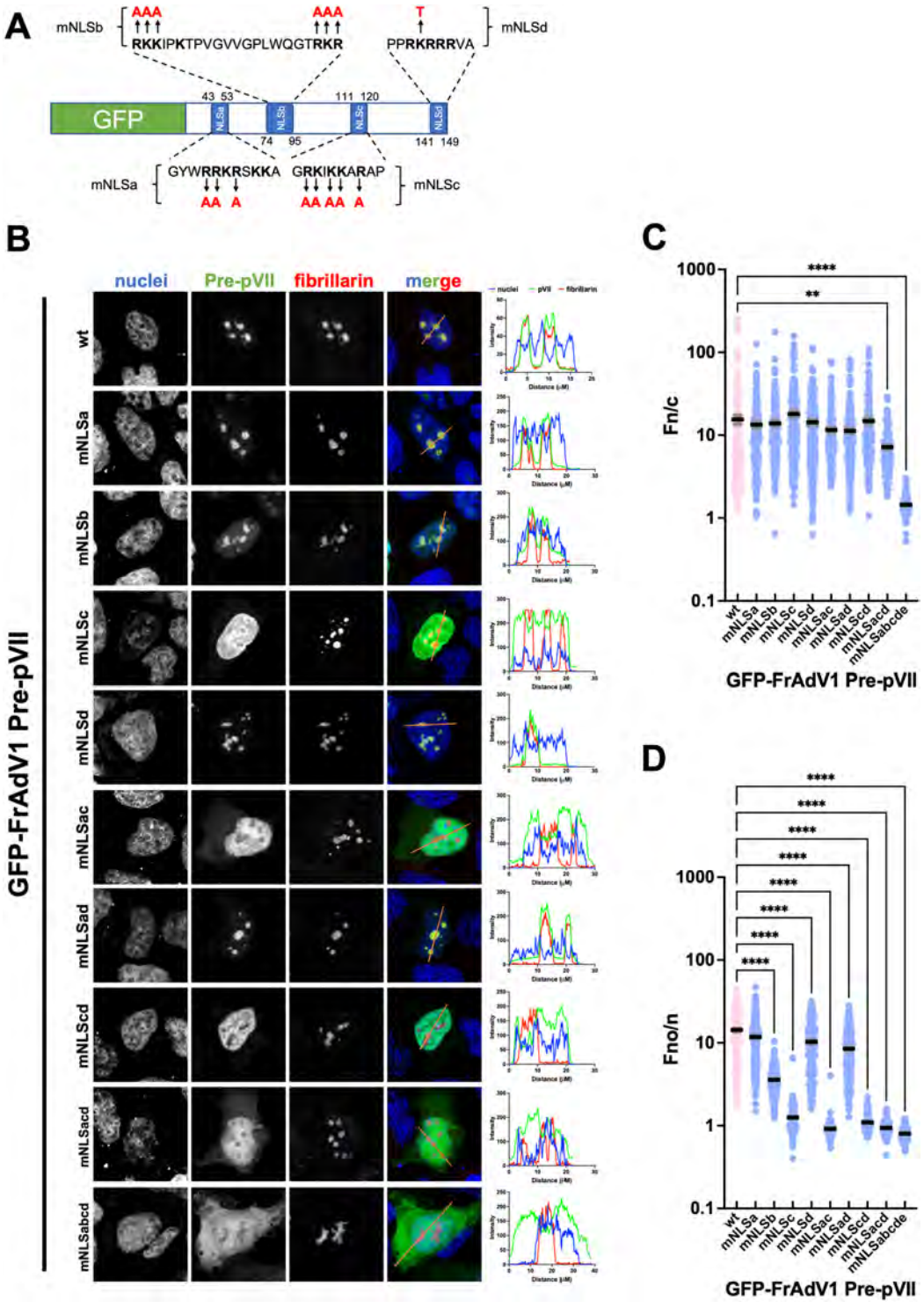

FIGURE 7 | Dissection of the individual contribution of each putative NLS to FrAdV1 nuclear and nucleolar targeting. (A) Schematic representation of the GFP-FrAdV1 Pre-pVII fusion proteins expressed. Proteins are represented by a *white horizontal bar*. NLSs are shown as *blue vertical bars*, along with their amino acidic sequence. Individual amino acidic substitutions are indicated by arrows and their sequence is in *red*. The *single letter* amino acid code is used. Basic residues are in *boldface*. (B) The indicated GFP fusion proteins were transiently co-expressed with DsRed-fibrillarin in HEK293A by means of Lipofectamine 2000 transfection. Twenty-four-hour post transfection, cells were incubated with DRAQ5 to stain cell nuclei, fixed with paraformaldehyde and processed for CLSM analysis as described in the Materials and Methods section. Representative images of the 633 nm (*nuclei*), 488 nm (*Pre-pVII*), and 561 nm (*fibrillarin*) laser channels are shown, along with a merged image (*merge*), and a rgb profile plot across the indicated area. (C, D) Micrographs such as those shown in (B) were quantitatively analyzed to calculate the levels of nuclear (C) or nucleolar (D) accumulation relative to the indicated fusion proteins at the single cell level, as described in the Materials and Methods section. Data shown are individual measurements (*circles*), along with means (*black horizontal bars*) ± standard error of the mean (SEM), relative to pooled data from at least 70 cells from three independent experiments. Results from Welch and Brown–Forsythe ANOVA test for accumulation of the indicated mutant Pre-pVII proteins as compared to the wild-type protein. $^{**}p < 0.01$; $^{****}p < 0.0001$.

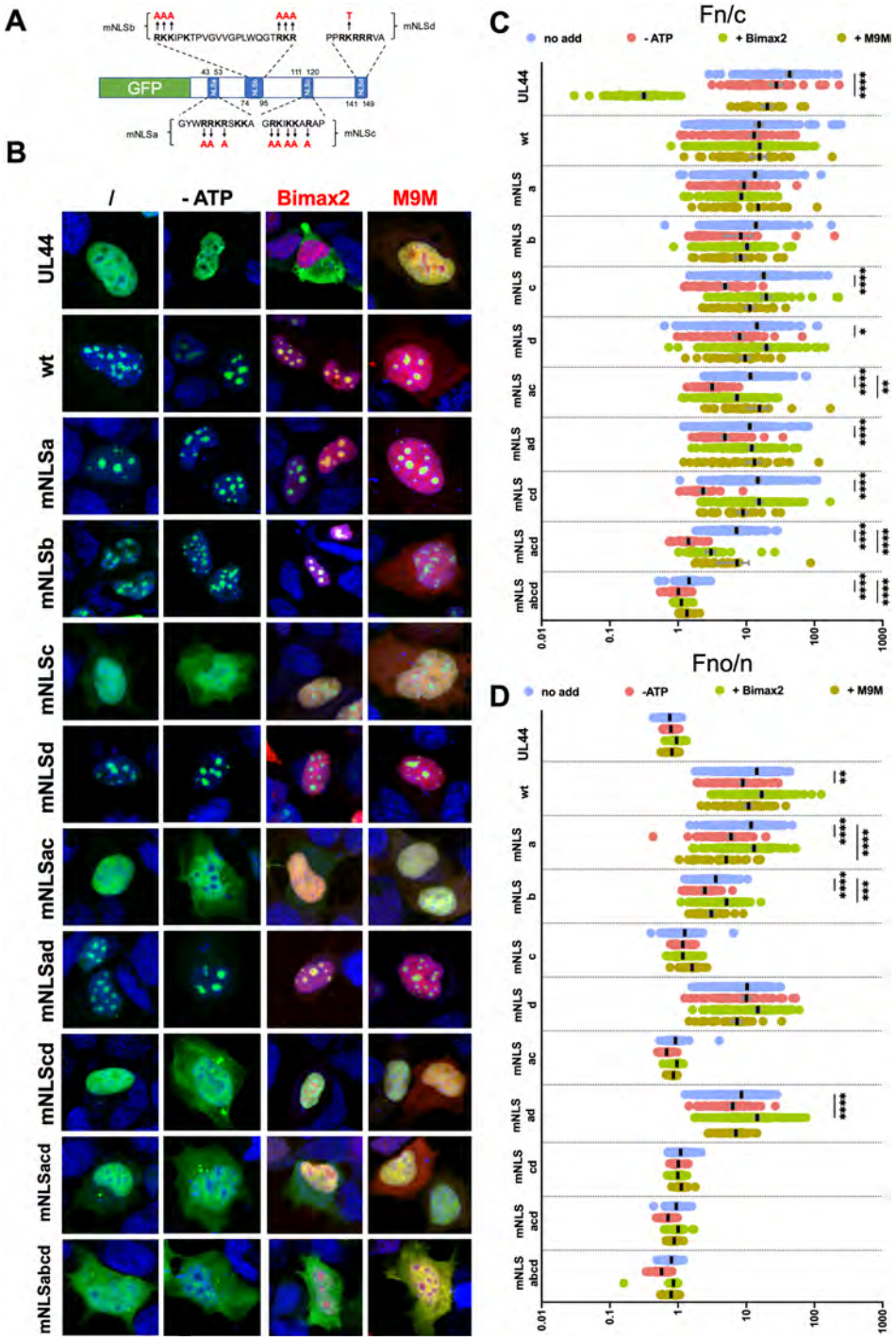

FIGURE 8 | Selective response of FrAdV1 Pre-pVII NLS substitution derivatives to nuclear transport inhibitors unveils the specific interaction of individual NLSs with cellular IMPs. (A) Schematic representation of the GFP-FrAdV1 Pre-pVII fusion proteins expressed. Proteins are represented by a *white horizontal bar*. NLSs are shown as *blue vertical bars*, along with their amino acidic sequence. Individual amino acidic substitutions are indicated by arrows, and their sequence is in *red*. The *single letter* amino acid code is used. Basic residues are in *boldface*. (B) The indicated GFP fusion proteins were transiently expressed in HEK293A by means of Lipofectamine 2000 transfection, in the absence (*no add*) or in the presence of plasmids mediating the expression of either mCherry-Bimax2 *(Bimax2*) or RFP-M9M *(M9M*). Twenty-four-hour post transfection, cells were incubated with DRAQ5 to stain cell nuclei, fixed with paraformaldehyde, and processed for CLSM analysis as described in the Materials and Methods section. Alternatively, cells were incubated for 30 min with 10 mmol/L sodium azide, 6 mmol/L 2-deoxy-D-glucose and DRAQ5, before being fixed with paraformalehyde and processed for CLSM analysis as above (-ATP). Representative merged images of 633 nm (*nuclei, blue*), 488 nm (*GFP, green*), and 561 nm (*inhibitors, red)* laser lines are shown. Images of individual channels and additional histograms are shown in the Figures S6–S12. (C, D) Micrographs such as those shown in (B) were quantitatively analyzed to calculate the levels of nuclear (C) or nucleolar (D) accumulation relative to the indicated fusion proteins at the single cell level, as described in the Materials and Methods section. Data shown are individual measurements (*circles*), along with are means (*black horizontal bars*) ± standard error of the mean (*SEM*), relative to pooled data from at least 20 cells from three independent experiments. Results from Welch and Brown–Forsythe ANOVA test for accumulation of the indicated GFP fusion protein expressed in the absence or in the presence of the indicated nuclear transport inhibitors. *$p < 0.05$; **$p < 0.01$; ***$p < 0.001$; ****$p < 0.0001$; ns, nonsignificant.

such as in the case of FrAdV1 Pre-pVII mNLSac, and Pre-pVII mNLSacd (Figure 8B,C and Figures S9 and S10), suggesting that when both NLSa (which directly interacts with IMPβ1) and NLSc (which tethers the protein in the nucleolus) are inactivated, FrAdV1 nuclear localization relies on IMPα/β1.

Intriguingly, M9M did not inhibit nuclear import of any FrAdV1 derivative (Figure 8 and Figures S11 and S12), despite the reduced accumulation of a GFP-GST-FUS fusion protein, which has been shown to be functionally depend on IMPβ2 (Figure S5CD). Therefore, IMPβ2 does not play a major role in FrAdV1 Pre-pVII nuclear import.

Taken together, our data suggest that each signal identified in this study plays a specific role in mediating FrAdV1 Pre-pVII subcellular trafficking. NLSa confers IMPβ1-dependent nuclear import, NLSb is an atypical sequence which contributes both to IMPα/β1 nuclear import and nucleolar targeting, and NLSc is the main NoLS, mediating nucleolar localization by interacting with intranuclear components, while NLSd is a cNLS conferring IMPα/β1 nuclear import.

4 | Discussion

The histone-like pVII core protein is suggested to be the major adaptor protein in DNA binding apart from its role in viral genome translocation, protecting the genome from host cellular DNA damage machinery, and virus assembly [1, 10]. Previous studies reported the ability of pVII to bind multiple import receptors and thereby access the transport machinery. Although several studies have identified NLSs in pVII from human mastadenovirus C and PsSiAdV [8, 12, 28], the presence, specific contribution, as well as their role in nuclear import of various other adenovirus members remained elusive. Here we have combined bioinformatics, microscopy imaging, biochemical and structural approaches to identify and characterize four putative NLSs in Pre-pVII from the ancient siadenovirus FrAdV1. Furthermore, by co-expression of wild type and NLS substitution derivatives thereof in the presence and absence of several nuclear import pathways inhibitors (Figures 2, 6, 7, and 8) we have characterized the contribution of each NLS to the subcellular localization of FrAdV1 Pre-pVII, thus unveiling the contribution of different nuclear import pathways and of intranuclear binding to its subcellular localization. Therefore, our study could provide a basis for future evolutionary comparisons regarding different AdV pVII proteins [8, 10, 12, 27].

Our findings strengthen the hypothesis that Pre-pVII from different AdVs are endowed with specific subcellular localization abilities. Indeed, when expressed in the absence of other viral proteins, FrAdV1 Pre-pVII strongly accumulated in cell nucleoli (Figure 2), in stark contrast to what was reported for Pre-pVII from PsSiAdV which is known to accumulate in the nucleoplasm [28], from HAdV2, which has been shown to localize in the nucleoplasm and in the nucleoli [8], and from BAdV-3 which localizes to mitochondria during viral infection [59]. The reason and functional significance for such discrepancies remain elusive, but it is noteworthy that in the case of FrAdV-1, nucleolar accumulation is dependent on a highly basic sequence (NLSc: $_{111}$G**RK**I**KK**A**R**AP$_{120}$), which is the main determinant of nucleolar targeting, and a bipartite sequence located upstream (NLSb: $_{74}$**RKK**IP**K**TPVGVVGPLWQGT**RKR**$_{95}$; see Figure 7), which also contributes to the process, although to a lesser extent. On the other hand, only one NoLS ($_{93}$M**RR**YA**K**MK**RRRRR**VA**RR**H**RRR**$_{112}$) has been identified in HAdV2 Pre-pVII [8], while none have been identified in PsSiAdV Pre-pVII [28]. Therefore, it is likely that the number and strength of NoLSs on AdV Pre-pVII proteins influences their degree of nucleolar targeting.

We propose a model for Frog Pre-pVII nuclear transport where the strong nucleolar targeting is due to the concerted action of the four signals identified here, each playing a specific role in protein subcellular localization. The *N*-terminal NLSa appears to be a nonclassical NLS, binding with high affinity to IMPβ1 directly (Figures 3 and 4), similarly to HIV-1 tat and Rev NLSs [60]. NLSb is poorly active outside of its physiological context, both in terms of IMP binding (Figure 3) and nuclear targeting activity (Figure 4 and Figures S2 and S3). However, it is sufficient to confer IMPα/β1 dependent nuclear targeting to full-length FrAdV1 Pre-pVII once all other NLSs have been inactivated (Figures 7 and 8). This suggest that NLSb might be an atypical NLS which binds IMPα/β1 thanks to its specific three-dimensional conformation, rather than in a liner fashion, such as reported for the NLS described in the intestinal fatty acid–binding protein [61]. NLSc can partially target GFP, but not the larger reporter GFP-β-gal to the nucleolus in an IMPα/β1 independent fashion, and does not bind either IMPα2 nor IMPβ1 with high affinity (Figure 3 and Table S3). However, substitution of its basic residues in the context of full-length Pre-pVII significantly impairs nucleolar targeting (Figure 7) and allows the protein to diffuse out of the nucleus once intracellular GTP is depleted by treatment of cells with sodium azide and 2-dexoxy-D glucose [57]. Therefore, NLSc is crucial for nucleolar localization, but, by itself, not sufficient to localize proteins to the nucleus, similarly to regions within HAdV2 that act as NoLS [8]. Finally, the C-terminal NLSd is a *bona fidae* monopartite cNLS, directly interacting with IMPα2 major binding site (Figures 3–5) and able to confer IMPα/β1 mediated nuclear import to heterologous proteins (Figure 2 and Figures S2 and S3). Importantly, only inactivation of all the four signals identified here completely ablated nuclear accumulation (Figure 7), in analogous fashion to what very recently reported for BAdV-3 Pre-pVII [13].

Therefore, our data are consistent with previous studies that reported the ability of Pre-pVII proteins to bind several IMPs and be imported through multiple pathways [8, 10, 12, 27]. Although HAdV2 Pre-pVII nuclear transport is dependent on IMPα/β1 [12], wild-type FrAdV1 Pre-pVII can accumulate in the nucleolus even in the presence of the highly efficient IMPα/β1 inhibitor Bimax2. Since simultaneous mutation of NLSc (conferring nucleolar accumulation) and NLSa (binding to IMPβ1 with high affinity) renders FrAdV1 Pre-pVII nuclear transport sensitive to Bimax2, FrAdV1 can be actively imported in the nucleus by IMPα/β1 (via NLSd) and IMPβ1 (via NLSa). However, we cannot rule out that FrAdV1 Pre-pVII can also interact with other IMPs for which well-characterized inhibitors are not available yet [17].

FrAdV1 Pre-pVII nuclear and nucleolar localization were not impacted by depletion of intracellular GTP, which is known to disrupt Ran-dependent active nuclear import, unless the highly

basic NLSc, which confers nucleolar localization, is inactivated (Figure 8). This strongly supports the idea that, once in the nucleus, FrAdV1 Pre-pVII can be therein retained after interaction with dsDNA and other nuclear components similarly to HAdV2 Pre-pVII which has been shown to interact with cellular DNA and co-localize with human chromosomes [8].

In conclusion, our findings revealed important differences between the import of FrAdV1 Pre-pVII in comparison to what has been reported for HAdV and PsSiAdV. In particular, the protein accumulated in the nucleolus more strongly as compared to its orthologs, and its nuclear targeting is insensitive to inhibition of IMPα/β1. The findings of this study provide valuable insights into how different adenoviruses interact with the host cell's nuclear transport machinery. Understanding these interactions may have broader implications for viral replication and infection strategies across different adenovirus genera and potential applications in therapeutic approaches.

Author Contributions

The authors' contributions include the following: conceptualization by A.A., B.P.M., J.K.F., G.A., and S.S.; experiments performed by A.A., S.N., B.N., S.P., and V.A.D.; data acquisition and analysis by A.A., S.N., C.M.D., and G.A.; writing of the initial draft by G.A., A.A., and S.N.; review and editing by A.A., C.M.D., S.P., S.N., V.A.D., B.N., K.J.H., B.P.M., G.A., J.K.F., S.S., and E.D.; supervision by G.A. and S.S.; and funding acquisition by S.S. All authors have read and agreed to the published version of the manuscript.

Acknowledgment

Open access publishing facilitated by Universita degli Studi di Padova, as part of the Wiley - CRUI-CARE agreement.

Ethics Statement

The authors have nothing to report.

Conflicts of Interest

The authors declare no conflicts of interest.

Data Availability Statement

The data that support the findings of this study are available from the corresponding author, G.A., upon reasonable request.

References

1. A. J. Davison, K. M. Wright, and B. Harrach, "DNA Sequence of Frog Adenovirus," *Journal of General Virology* 81 (2000): 2431–2439.

2. E. R. Kovács and M. Benko, "Complete Sequence of Raptor Adenovirus 1 Confirms the Characteristic Genome Organization of Siadenoviruses," *Infection, Genetics and Evolution* 11, no. 5 (2011): 1058–1065.

3. M. Benko, K. Aoki, N. Arnberg, et al., "ICTV Virus Taxonomy Profile: Adenoviridae 2022," *Journal of General Virology* 103, no. 3 (2022).

4. T. H. Nguyen, M. Z. Ballmann, H. T. Do, et al., "Crystal Structure of Raptor Adenovirus 1 Fibre Head and Role of the Beta-Hairpin in Siadenovirus Fibre Head Domains," *Virology Journal* 13 (2016): 106.

5. A. K. Singh, M. A. Berbís, M. Z. Ballmann, et al., "Structure and Sialyllactose Binding of the Carboxy-Terminal Head Domain of the Fibre From a Siadenovirus, Turkey Adenovirus 3," *PLoS One* 10, no. 9 (2015): e0139339.

6. B. Harrach, Z. L. Tarjan, and M. Benko, "Adenoviruses Across the Animal Kingdom: A Walk in the Zoo," *FEBS Letters* 593, no. 24 (2019): 3660–3673.

7. A. Athukorala, D. N. Phalen, A. Das, K. J. Helbig, J. K. Forwood, and S. Sarker, "Genomic Characterisation of a Highly Divergent Siadenovirus (Psittacine Siadenovirus F) From the Critically Endangered Orange-Bellied Parrot (Neophema Chrysogaster)," *Viruses* 13, no. 9 (2021).

8. T. W. R. Lee, G. E. Blair, and D. A. Matthews, "Adenovirus Core Protein VII Contains Distinct Sequences That Mediate Targeting to the Nucleus and Nucleolus, and Colocalization With Human Chromosomes," *Journal of General Virology* 84, no. Pt 12 (2003): 3423–3428.

9. T. J. Wickham, P. Mathias, D. A. Cheresh, and G. R. Nemerow, "Integrins Alpha v Beta 3 and Alpha v Beta 5 Promote Adenovirus Internalization But Not Virus Attachment," *Cell* 73, no. 2 (1993): 309–319.

10. H. Wodrich, A. Cassany, M. A. D'Angelo, T. Guan, G. Nemerow, and L. Gerace, "Adenovirus Core Protein pVII Is Translocated Into the Nucleus by Multiple Import Receptor Pathways," *Journal of Virology* 80, no. 19 (2006): 9608–9618.

11. U. F. Greber and M. Suomalainen, "Adenovirus Entry: Stability, Uncoating, and Nuclear Import," *Molecular Microbiology* 118, no. 4 (2022): 309–320.

12. C. E. Hindley, F. J. Lawrence, and D. A. Matthews, "A Role for Transportin in the Nuclear Import of Adenovirus Core Proteins and DNA," *Traffic* 8, no. 10 (2007): 1313–1322.

13. S. Kulanayake, F. Dar, and S. K. Tikoo, "Regions of Bovine Adenovirus-3 Protein VII Involved in Interactions With Viral and Cellular Proteins," *Viruses* 16, no. 5 (2024).

14. B. L. Timney, B. Raveh, R. Mironska, et al., "Simple Rules for Passive Diffusion Through the Nuclear Pore Complex," *Journal of Cell Biology* 215, no. 1 (2016): 57–76.

15. D. Gorlich, S. Kostka, R. Kraft, et al., "Two Different Subunits of Importin Cooperate to Recognize Nuclear Localization Signals and Bind Them to the Nuclear Envelope," *Current Biology* 5, no. 4 (1995): 383–392.

16. A. J. O'Reilly, J. B. Dacks, and M. C. Field, "Evolution of the Karyopherin-Beta Family of Nucleocytoplasmic Transport Factors; Ancient Origins and Continued Specialization," *PLoS One* 6, no. 4 (2011): e19308.

17. C. E. Wing, H. Y. J. Fung, and Y. M. Chook, "Karyopherin-Mediated Nucleocytoplasmic Transport," *Nature Reviews. Molecular Cell Biology* 23, no. 5 (2022): 307–328.

18. M. Soniat and Y. M. Chook, "Nuclear Localization Signals for Four Distinct Karyopherin-Beta Nuclear Import Systems," *Biochemical Journal* 468, no. 3 (2015): 353–362.

19. E. Conti, M. Uy, L. Leighton, G. Blobel, and J. Kuriyan, "Crystallographic Analysis of the Recognition of a Nuclear Localization Signal by the Nuclear Import Factor Karyopherin Alpha," *Cell* 94, no. 2 (1998): 193–204.

20. C. Dingwall, J. Robbins, S. M. Dilworth, B. Roberts, and W. D. Richardson, "The Nucleoplasmin Nuclear Location Sequence Is Larger and More Complex Than That of SV-40 Large T Antigen," *Journal of Cell Biology* 107, no. 3 (1988): 841–849.

21. D. Kalderon, W. D. Richardson, A. F. Markham, and A. E. Smith, "Sequence Requirements for Nuclear Location of Simian Virus 40 Large-T Antigen," *Nature* 311, no. 5981 (1984): 33–38.

22. G. Alvisi, D. A. Jans, D. Camozzi, et al., "Regulated Transport Into the Nucleus of Herpesviridae DNA Replication Core Proteins," *Viruses* 5, no. 9 (2013): 2210–2234.

23. G. Cingolani, J. Bednenko, M. T. Gillespie, and L. Gerace, "Molecular Basis for the Recognition of a Nonclassical Nuclear Localization Signal by Importin Beta," *Molecular Cell* 10, no. 6 (2002): 1345–1353.

24. M. R. Fontes, T. Teh, and B. Kobe, "Structural Basis of Recognition of Monopartite and Bipartite Nuclear Localization Sequences by Mammalian Importin-Alpha," *Journal of Molecular Biology* 297, no. 5 (2000): 1183–1194.

25. J. Kalita, L. E. Kapinos, and R. Y. H. Lim, "On the Asymmetric Partitioning of Nucleocytoplasmic Transport – Recent Insights and Open Questions," *Journal of Cell Science* 134, no. 7 (2021).

26. D. Gorlich, N. Pante, U. Kutay, U. Aebi, and F. R. Bischoff, "Identification of Different Roles for RanGDP and RanGTP in Nuclear Protein Import," *EMBO Journal* 15, no. 20 (1996): 5584–5594.

27. S. Kulanayake and S. K. Tikoo, "Adenovirus Core Proteins: Structure and Function," *Viruses* 13, no. 3 (2021).

28. A. Athukorala, C. M. Donnelly, S. Pavan, et al., "Structural and Functional Characterization of Siadenovirus Core Protein VII Nuclear Localization Demonstrates the Existence of Multiple Nuclear Transport Pathways," *Journal of General Virology* 105, no. 1 (2024).

29. S. Kosugi, M. Hasebe, T. Entani, S. Takayama, M. Tomita, and H. Yanagawa, "Design of Peptide Inhibitors for the Importin Alpha/Beta Nuclear Import Pathway by Activity-Based Profiling," *Chemistry & Biology* 15, no. 9 (2008): 940–949.

30. J. Jumper, R. Evans, A. Pritzel, et al., "Highly Accurate Protein Structure Prediction With AlphaFold," *Nature* 596, no. 7873 (2021): 583–589.

31. M. Hoad, E. M. Cross, C. M. Donnelly, S. Sarker, J. A. Roby, and J. K. Forwood, "Structural Characterization of Porcine Adeno-Associated Virus Capsid Protein With Nuclear Trafficking Protein Importin Alpha Reveals a Bipartite Nuclear Localization Signal," *Viruses* 15, no. 2 (2023).

32. T. Teh, T. Tiganis, and B. Kobe, "Crystallization of Importin Alpha, the Nuclear-Import Receptor," *Acta Crystallographica Section D, Biological Crystallography* 55, no. Pt 2 (1999): 561–563.

33. G. Alvisi, E. Manaresi, E. M. Cross, et al., "Importin Alpha/Beta-Dependent Nuclear Transport of Human Parvovirus B19 Nonstructural Protein 1 Is Essential for Viral Replication," *Antiviral Research* 213 (2023): 105588.

34. E. Sinigalia, G. Alvisi, B. Mercorelli, et al., "Role of Homodimerization of Human Cytomegalovirus DNA Polymerase Accessory Protein UL44 in Origin-Dependent DNA Replication in Cells," *Journal of Virology* 82, no. 24 (2008): 12574–12579.

35. D. Dormann, T. Madl, C. F. Valori, et al., "Arginine Methylation Next to the PY-NLS Modulates Transportin Binding and Nuclear Import of FUS," *EMBO Journal* 31, no. 22 (2012): 4258–4275.

36. A. Gomez Corredor and D. Archambault, "The Bovine Immunodeficiency Virus Rev Protein: Identification of a Novel Lentiviral Bipartite Nuclear Localization Signal Harboring an Atypical Spacer Sequence," *Journal of Virology* 83, no. 24 (2009): 12842–12853.

37. Y. Kino, C. Washizu, E. Aquilanti, et al., "Intracellular Localization and Splicing Regulation of FUS/TLS Are Variably Affected by Amyotrophic Lateral Sclerosis-Linked Mutations," *Nucleic Acids Research* 39, no. 7 (2011): 2781–2798.

38. A. Tsujii, Y. Miyamoto, T. Moriyama, et al., "Retinoblastoma-Binding Protein 4-Regulated Classical Nuclear Transport Is Involved in Cellular Senescence," *Journal of Biological Chemistry* 290, no. 49 (2015): 29375–29388.

39. G. Sorg and T. Stamminger, "Mapping of Nuclear Localization Signals by Simultaneous Fusion to Green Fluorescent Protein and to Beta-Galactosidase," *BioTechniques* 26, no. 5 (1999): 858–862.

40. G. Alvisi, D. Jans, J. Guo, L. Pinna, and A. Ripalti, "A Protein Kinase CK2 Site Flanking the Nuclear Targeting Signal Enhances Nuclear Transport of Human Cytomegalovirus ppUL44," *Traffic* 6, no. 11 (2005): 1002–1013.

41. N. Roman, M. Christie, C. M. Swarbrick, B. Kobe, and J. K. Forwood, "Structural Characterisation of the Nuclear Import Receptor Importin Alpha in Complex With the Bipartite NLS of Prp20," *PLoS One* 8, no. 12 (2013): e82038.

42. F. W. Studier, "Protein Production by Auto-Induction in High Density Shaking Cultures," *Protein Expression and Purification* 41, no. 1 (2005): 207–234.

43. E. M. Cross, N. Akbari, H. Ghassabian, et al., "A Functional and Structural Comparative Analysis of Large Tumor Antigens Reveals Evolution of Different Importin Alpha-Dependent Nuclear Localization Signals," *Protein Science* 33, no. 2 (2024): e4876.

44. E. M. Cross, O. Marin, D. Ariawan, et al., "Structural Determinants of Phosphorylation-Dependent Nuclear Transport of HCMV DNA Polymerase Processivity Factor UL44," *FEBS Letters* 598, no. 2 (2024): 199–209.

45. D. Aragao, J. Aishima, H. Cherukuvada, et al., "MX2: A High-Flux Undulator Microfocus Beamline Serving Both the Chemical and Macromolecular Crystallography Communities at the Australian Synchrotron," *Journal of Synchrotron Radiation* 25, no. Pt 3 (2018): 885–891.

46. W. Kabsch, "Xds," *Acta Crystallographica Section D, Biological Crystallography* 66, no. Pt 2 (2010): 125–132.

47. P. R. Evans, "An Introduction to Data Reduction: Space-Group Determination, Scaling and Intensity Statistics," *Acta Crystallographica Section D* 67 (2011): 282–292.

48. P. Emsley, B. Lohkamp, W. G. Scott, and K. Cowtan, "Features and Development of Coot," *Acta Crystallographica Section D, Biological Crystallography* 66, no. Pt 4 (2010): 486–501.

49. P. D. Adams, P. V. Afonine, G. Bunkoczi, et al., "PHENIX: A Comprehensive Python-Based System for Macromolecular Structure Solution," *Acta Crystallographica Section D, Biological Crystallography* 66, no. Pt 2 (2010): 213–221.

50. A. J. McCoy, R. W. Grosse-Kunstleve, P. D. Adams, M. D. Winn, L. C. Storoni, and R. J. Read, "Phaser Crystallographic Software," *Journal of Applied Crystallography* 40, no. Pt 4 (2007): 658–674.

51. E. Krissinel and K. Henrick, "Inference of Macromolecular Assemblies From Crystalline State," *Journal of Molecular Biology* 372, no. 3 (2007): 774–797.

52. L. Messa, M. Celegato, C. Bertagnin, et al., "The Dimeric Form of HPV16 E6 Is Crucial to Drive YAP/TAZ Upregulation Through the Targeting of hScrib," *Cancers* 13, no. 16 (2021).

53. V. Di Antonio, G. Palu, and G. Alvisi, "Live-Cell Analysis of Human Cytomegalovirus DNA Polymerase Holoenzyme Assembly by Resonance Energy Transfer Methods," *Microorganisms* 9, no. 5 (2021).

54. G. Alvisi, D. Jans, and A. Ripalti, "Human Cytomegalovirus (HCMV) DNA Polymerase Processivity Factor ppUL44 Dimerizes in the Cytosol Before Translocation to the Nucleus," *Biochemistry* 45, no. 22 (2006): 6866–6872.

55. G. Alvisi, L. Paolini, A. Contarini, et al., "Intersectin Goes Nuclear: Secret Life of an Endocytic Protein," *Biochemical Journal* 475, no. 8 (2018): 1455–1472.

56. K. M. Smith, V. Di Antonio, L. Bellucci, et al., "Contribution of the Residue at Position 4 Within Classical Nuclear Localization Signals to Modulating Interaction With Importins and Nuclear Targeting," *Biochimica et Biophysica Acta* 1865, no. 8 (2018): 1114–1129.

57. E. D. Schwoebel, T. H. Ho, and M. S. Moore, "The Mechanism of Inhibition of Ran-Dependent Nuclear Transport by Cellular ATP Depletion," *Journal of Cell Biology* 157, no. 6 (2002): 963–974.

58. G. Alvisi, S. Avanzi, D. Musiani, et al., "Nuclear Import of HSV-1 DNA Polymerase Processivity Factor UL42 Is Mediated by a C-Terminally Located Bipartite Nuclear Localization Signal," *Biochemistry* 47, no. 52 (2008): 13764–13777.

59. S. K. Anand, A. Gaba, J. Singh, and S. K. Tikoo, "Bovine Adenovirus 3 Core Protein Precursor pVII Localizes to Mitochondria, and Modulates ATP Synthesis, Mitochondrial Ca^{2+} and Mitochondrial Membrane Potential," *Journal of General Virology* 95 (2014): 442–452.

60. Y. M. Chook and K. E. Suel, "Nuclear Import by Karyopherin-Betas: Recognition and Inhibition," *Biochimica et Biophysica Acta* 1813, no. 9 (2011): 1593–1606.

61. M. Suarez, L. Canclini, and A. Esteves, "Identification of a Non-Classical Three-Dimensional Nuclear Localization Signal in the Intestinal Fatty Acid Binding Protein," *PLoS One* 15, no. 11 (2020): e0242312.

Supporting Information

Additional supporting information can be found online in the Supporting Information section.